Nuclear reaction cross sections from a simple effective density using a Glauber model

Mahesh K. Sharma[1,2] and S. K. Patra[3]
[1]*Department of Applied Science, Chandigarh Engineering College, Landran, Mohali 140307, India*
[2]*School of Physics and Materials Science, Thapar University, Patiala 147004, India*
[3]*Institute of Physics, Sahcivalya Marg, Bhubaneswar 751005, India*
(Received 18 December 2012; revised manuscript received 22 February 2013; published 10 April 2013)

We have studied the nuclear reaction dynamics of few halo nuclei in the framework of the well-known Glauber formalism using relativistic (NL3) and nonrelativistic (SEI-I) densities. We find reasonably good agreement with the experimental data of reaction cross sections. A further careful inspection of the results shows that the SEI-I density reproduces better results as compared to the NL3 results.

DOI: 10.1103/PhysRevC.87.044606 PACS number(s): 25.70.Jj, 25.60.Pj, 24.10.−i, 27.30.+t

I. INTRODUCTION

In recent years, the study of exotic nuclei has attracted considerable theoretical and experimental attention. With the advancements in the radioactive ion beam facilities, it has become possible to perform numerous experiments to get more information regarding the structures of such nuclei. Neutron and proton halos, Borromean structure, neutron skin, and bubble structure are some of the current issues of interest. The most exotic phenomenon is the formation of a neutron halo by the extremely weak bound neutrons that decouple from the nuclear core. The interaction cross sections of nuclei like ^{6,8}He, ^{11}Li, and ^{11,14}Be [1,2] have been found to be anomalously larger values due to their respective large root-mean-square (rms) radii. The investigation of large matter radii and interaction cross sections for ^{19}C, ^{22}N, ^{23}O, and ^{24}F suggest the feature of one-neutron halo nuclei [3].

Recently, a new member ^{31}Ne has been included in the family of neutron halos [4]. The isotope ^{31}Ne having $N = 21$ breaks the shell closer structure and, as a consequence, a large amount of deformation gets associated with the strong intruder configuration. Eventually this nuclear system lies at the island of inversion [5]. The measurement of nuclear reaction cross section for ^{19,20,22}C [6,7] shows that the drip-line nucleus ^{22}C has a halo. The one- and two-neutron removal cross sections and momentum distribution are used to get an indication of the existence of halo nuclei. ^{22}C has $N = 16$ which is a new magic number in neutron-rich nuclei [8,9] and forms a Borromean halo structure (^{21}C is unstable). Therefore, these are the points that motivate us to study the reaction dynamics of such halo candidates. Second, the successful development of simple effective interaction (SEI) [10] encourages us to use the formalism for such systems. In our recent publication [11], we have shown that the density obtained from the relativistic mean-field (RMF) approximation in the framework of the Glauber model predicts the nuclear reaction cross section σ_R much closer to the experimental data. Although, it is known that the mean-field approaches do not reproduce the halo structure of nuclei quantitatively, it predicts the drip-line properties quite well even for the light nuclei region. Thus, it is instructive to use the SEI densities and calculate σ_R for such interesting systems and compare the results with the known RMF(NL3) formalism [12].

This paper is organized as follows. Section II contains a brief description of the Glauber model, the SEI formalism, and the RMF theory. The calculations and results are presented in Sec. III. Here, the ground-state properties like binding energy, rms radii, and density distribution are evaluated in the framework of the RMF and SEI formalisms. Then the total reaction cross section σ_R is estimated for some of the selected exotic nuclei. Finally the summary and conclusions are outlined in Sec. IV.

II. THE FORMALISM

We use the well-known Glauber approach (core + one nucleon) to investigate reaction dynamics [13,14]. This approach strongly depends on the densities of the projectile and target nuclei. We use the axially deformed microscopic RMF densities with the NL3 parameters [12] and the density obtained by the recently proposed SEI parametrizations [10]. The details about the formalism and interaction parameters can be found in Refs. [13–16], [12,17–19], and [10] for the Glauber, RMF, and SEI models, respectively. For completeness, the essential features of these formalisms are outlined in Secs. II A, II B, and II C.

A. Glauber model

1. Reaction cross section

The theoretical formalism to study the reaction cross sections using the Glauber approach has been given by Glauber [13]. The nucleus-nucleus elastic scattering amplitude is written as

$$F(q) = \frac{\iota K}{2\pi} \int dbe^{-\iota\cdot q\cdot b}(1 - e^{\iota\chi(b)}). \tag{1}$$

At low energy, this model is modified to take care of finite range effects in the profile function and Coulomb-modified trajectories. The elastic scattering amplitude including the Coulomb interaction is expressed as

$$F(q) = e^{\iota\chi_s}\left\{F_{\rm Coul}(q) + \frac{\iota K}{2\pi}\int dbe^{-\iota\cdot q\cdot b+2\iota\eta\ln(Kb)}(1 - e^{\iota\chi(b)})\right\}, \tag{2}$$

with the Coulomb elastic scattering amplitude

$$F_{\rm Coul}(q)=\frac{-2\eta K}{q^2}\exp\left\{-2\iota\eta\ln\left(\frac{q}{2K}\right)+2\iota\arg\Gamma(1+\iota\eta)\right\}, \tag{3}$$

where K is the momentum of the projectile and q is the momentum transferred from the projectile to the target. Here $\eta = Z_P Z_T e^2/\hbar v$ is the Sommerfeld parameter, v is the incident velocity of the projectile, and $\chi_s = -2\eta\ln(2Ka)$, with a being a screening radius. The elastic differential cross section is given by

$$\frac{d\sigma}{d\Omega} = |F(q)|^2. \tag{4}$$

The standard Glauber form for total reaction cross sections is expressed as [13,15]

$$\sigma_R = 2\pi\int_0^\infty b[1-T(b)]db, \tag{5}$$

where $T(b)$ is the transparency function with impact parameter b. The function $T(b)$ can be expressed in terms of the phase shift function by

$$T(b) = e^{|\iota\chi_{\rm PT}(b)|^2}. \tag{6}$$

Here, $\chi_{\rm PT}$ is the projectile-target phase shift function. The phase shift function has been expressed for the two-body (core + neutron) projectile system as

$$\iota\chi_{\rm PT}(b) = \iota\chi_{\rm CT}(b) + \iota\chi_{\rm NT}(b), \tag{7}$$

where

$$\iota\chi_{\rm CT}(b) = -\int_p\int_t\sum_{i,j}\Gamma_{ij}(\vec{b}-\vec{s}+\vec{s'}) \times\overline{\rho}_{pi}(\vec{s'})\overline{\rho}_{tj}(\vec{s})\vec{ds}\vec{ds'}, \tag{8}$$

and

$$\iota\chi_{\rm NT}(b) = -\int_t\Gamma_{ij}(\vec{b}-\vec{s})\overline{\rho}_{tj}(\vec{s})\vec{ds}. \tag{9}$$

The profile function Γ_{NN} for the optical limit approximation is defined as

$$\Gamma_{NN} = \Gamma_{ij}(b_{\rm eff}) = \frac{1-\iota\alpha_{NN}}{2\pi\beta_{NN}^2}\sigma_{NN}\exp\left(-\frac{b_{\rm eff}^2}{2\beta_{NN}^2}\right) \tag{10}$$

for the finite range and

$$\Gamma_{NN} = \Gamma_{ij}(b_{\rm eff}) = \frac{1-\iota\alpha_{NN}}{2}\sigma_{NN}\delta(b) \tag{11}$$

for the zero range, where $b_{\rm eff} = |\vec{b}-\vec{s}+\vec{s'}|$, $\vec{b}$ is the impact parameter, and $\vec{s}$ and $\vec{s'}$ are the projections of intrinsic coordinates of projectile and target densities, respectively, onto the impact parameter plane. The z-integrated densities are defined as

$$\overline{\rho}(\omega) = \int_{-\infty}^{\infty}\rho(\sqrt{w^2+z^2})dz, \tag{12}$$

with $\omega^2 = x^2+y^2$. Initially the Glauber model was designed for the high-energy approximation. However it was found to work reasonably well for both the nucleus-nucleus reaction and the differential elastic cross sections over a broad energy range [16]. The parameters σ_{NN}, α_{NN}, and β_{NN} are usually dependent upon the proton-proton, neutron-neutron, and proton-neutron interactions. It should be noted that these parameters which are used exclusively in the Glauber model are entirely independent and the input densities are obtained from two completely different formalisms.

B. Hartree-Fock with simple effective interactions

The SEI similar to Gogny is used to study the bulk properties of finite nuclei within the framework of the Hartree-Fock (HF) formalism. The form of SEI is given by [10]

$$\begin{aligned}v_{\rm eff}(r) &= t_0(1+x_0P_\sigma)\delta(r)\\ &+t_3(1+x_3P_\sigma)\left(\frac{\rho(R)}{1+b\rho(R)}\right)^\gamma\delta(r)\\ &+(W+BP_\sigma-HP_\tau-MP_\sigma P_\tau)f(r),\end{aligned} \tag{13}$$

where $f(r)$ is the functional form of the finite range interaction in term of the Gaussian function $f(r) = e^{-r^2/\alpha^2}$, which contains a single range parameter α. The other terms have their usual meaning [10].

The Hamiltonian density functional using the SEI [Eq. (13)] is written as

$$\mathcal{H} = \mathcal{K}+\mathcal{H}^{\rm Nucl}+\mathcal{H}^{\rm SO}(\mathbf{r})+\mathcal{H}^{\rm Coul}(\mathbf{r})+\mathcal{H}^{\rm RC}, \tag{14}$$

where $\mathcal{K} = \frac{\hbar^2}{2m}(\tau_n+\tau_p)$ is the kinetic energy term, with τ_n and τ_p being the proton and neutron kinetic energy densities of the nucleus. The second term of the Hamiltonian is the nuclear contribution, which contains the direct and exchange parts. The direct contribution of the nuclear energy density comes from the central part of the effective interaction. The third term is the spin-orbit interaction, written as

$$\mathcal{H}^{\rm SO}(\mathbf{r}) = \frac{-1}{2}W_0[\rho(\mathbf{r})\nabla\mathbf{J}+\rho_n(\mathbf{r})\nabla\mathbf{J}_n+\rho_p(\mathbf{r})\nabla\mathbf{J}_p]. \tag{15}$$

The fourth term is due to the Coulomb interaction, which contains both direct and exchange terms given as [10]

$$\mathcal{H}^{\rm Coul}(\mathbf{r}) = \frac{1}{2}\int\frac{\rho_p(\acute{\mathbf{r}})}{|\mathbf{r}-\acute{\mathbf{r}}|}d^3\acute{r}-\frac{3}{4}\left(\frac{3}{\pi}\right)^{1/3}\rho_p^{4/3}. \tag{16}$$

The last term of the equation arises from the zero range part of the SEI, which plays the role of residual correlation energy:

$$\begin{aligned}\mathcal{H}^{\rm RC} &= \frac{t_0}{4}\int\left\{(1-x_0)\left[\rho_n^2(\mathbf{r})+\rho_p^2(\mathbf{r})\right]\right\}\\ &+\frac{t_0}{4}\int[(4+2x_0)\rho_n(\mathbf{r})\rho_p(\mathbf{r})]\\ &+\frac{t_3}{24}\int\left\{(1-x_3)\left[\rho_n^2(\mathbf{r})+\rho_p^2(\mathbf{r})\right]\right\}\\ &+\frac{t_3}{24}\int[(4+2x_3)\rho_n(\mathbf{r})\rho_p(\mathbf{r})]\left(\frac{\rho(\mathbf{r})}{1+b\rho(\mathbf{r})}\right)^\gamma.\end{aligned} \tag{17}$$

Here ρ_n, ρ_p, ρ, J_n, J_p, and J are the neutron, proton, and total nuclear and current densities, respectively. The 12 parameters

TABLE I. The ground-state properties of projectile and target nuclei obtained from the RMF(NL3) and HF(SEI-I) calculations are compared with experimental data wherever available. The difference between the experimental and calculated binding energy, ΔB.E.$_{\rm RMF}$ and ΔB.E.$_{\rm HF}$, for RMF and HF, respectively, are given. The binding energy (B.E.) is in MeV, and $r_{\rm rms}$ and r_c are in fm.

Nuclei	B.E.			ΔB.E.	ΔB.E.	$r_{\rm rms}$		r_c			β_2
	RMF	HF(SEI)	Expt. [22,23]	RMF	HF(SEI)	RMF	HF(SEI)	RMF	HF(SEI)	Expt. [24]	RMF
^{12}C	89.761	88.422	92.160 ± 1.7	2.399	3.738	2.554	2.413	2.696	2.436	2.47(00)	0.068
^{4}He	34.466	29.003	28.292 ± 0.000	−6.174	−0.711	1.965	1.881	2.128	1.900	1.68(00)	0.011
^{5}He	33.692	31.314	27.560 ± 0.02	−6.132	−3.754	2.618	2.139	2.513	1.917		0.250
^{6}He	34.332	33.144	29.270 ± 0.042	−5.062	−3.874	2.411	2.296	2.100	1.926	2.07(01)	0.689
^{10}Li	52.663	51.107	45.130 ± 0.01	−7.533	−5.977	2.609	2.661	2.347	2.197		0.028
^{11}Li	54.585	52.737	45.709 ± 0.001	−8.876	−7.028	2.700	2.661	2.356	2.226	2.48(04)	0.019
^{10}Be	65.403	62.561	64.970 ± 0.08	2.409	2.587	2.600	2.379	2.588	2.286	2.36(02)	0.384
^{11}Be	67.954	69.380	65.472 ± 0.000	−2.482	−3.908	2.541	2.510	2.449	2.330	2.46(02)	0.366
^{14}C	107.348	105.829	105.280 ± 0.00	−2.068	−0.549	2.645	2.551	2.647	2.470	2.56(5)	0.025
^{15}C	108.719	108.846	106.500 ± 0.000	−2.219	−2.346	2.627	2.643	2.536	2.480		0.217
^{18}C	116.928	116.707	115.280 ± 0.306	−1.648	−1.427	2.909	2.859	2.616	2.509		0.437
^{19}C	119.655	119.015	116.242 ± 0.098	−3.413	−2.773	2.983	2.920	2.631	2.521		−0.432
^{21}C	121.630	123.096	119.154 ± 0.399	−2.476	−3.942	3.075	3.052	2.586	2.544		0.142
^{22}C	124.157	124.770	120.736 ± 0.506	−3.421	−4.034	3.111	3.133	2.580	2.557		0.016
^{22}O	163.353	164.763	162.008 ± 0.044	−1.345	−2.755	2.924	2.909	2.737	2.678		0.007
^{23}O	167.328	169.040	164.749 ± 0.090	−2.579	−4.291	2.961	2.973	2.726	2.689		−0.015
^{30}Ne	216.040	214.160	211.260 ± 0.270	−4.78	−2.900	3.260	3.236	2.996	2.933		0.004
^{31}Ne	216.145	214.569	211.544 ± 1.619	−4.601	−3.025	3.336	3.289	3.026	2.944		0.236

γ, b, t_0, t_3, x_0, x_3, W, B, H, M, α, and W_0 are used for the calculation of ground-state properties. The detailed procedure of calculations of ground-state properties (like binding energy, charge radius, nuclear matter radius, etc., and parameters' evaluation) in the HF approximation can be found in Ref. [10]. The values of parameters for SEI-I interactions are $\gamma = \frac{1}{2}$, $b = 0.5914$ fm^3, $t_0 = 437.0$ MeV fm^3, $t_3 = 9955.2$ MeV fm$^{3(\gamma+1)}$, $x_0 = 0.6$, $x_3 = -0.118$, $W = -589.09$ MeV, $B = 130.36$ MeV, $H = -272.42$ MeV, $M = -192.16$ MeV, $\alpha = 0.7596$ fm, and $W_0 = 115.0$ MeV.

C. Relativistic mean-field densities

The RMF approach is well documented in Refs. [17–21]. The basic ingredient of the RMF model is the relativistic Lagrangian density for a nucleon-meson many-body system, which is defined as [20]

$$\begin{aligned}\mathcal{L} = {} & \overline{\psi}_i(i\gamma^\mu\partial_\mu - M)\psi_i + \frac{1}{2}\partial^\mu\sigma\,\partial_\mu\sigma \\ & - \frac{1}{2}m_\sigma^2\sigma^2 - \frac{1}{3}g_2\sigma^3 - \frac{1}{4}g_3\sigma^4 - g_s\overline{\psi}_i\psi_i\sigma \\ & - \frac{1}{4}\Omega^{\mu\nu}\Omega_{\mu\nu} + \frac{1}{2}m_w^2V^\mu V_\mu \\ & - g_\omega\overline{\psi}_i\gamma^\mu\psi_i V_\mu - \frac{1}{4}\vec{B}^{\mu\nu}\cdot\vec{B}_{\mu\nu} \\ & + \frac{1}{2}m_\rho^2\vec{R}^\mu\cdot\vec{R}_\mu - g_\rho\overline{\psi}_i\gamma^\mu\vec{\tau}\psi_i\cdot\vec{R^\mu} \\ & - \frac{1}{4}F^{\mu\nu}F_{\mu\nu} - e\overline{\psi}_i\gamma^\mu\frac{(1-\tau_{3i})}{2}\psi_i A_\mu. \end{aligned} \quad (18)$$

Here σ, V_μ, and $\vec{R}_\mu$ are the fields for σ, ω, and ρ mesons, respectively. A^μ is the electromagnetic field. The ψ_i are

TABLE II. The one-neutron (S_n) and two-neutron (S_{2n}) separation energies along with single-particle (ε_n) energy values of halo nuclei obtained by the nonrelativistic HF(SEI-I) and RMF(NL3) formalisms. The values of S_n, S_{2n}, and ε_n are in MeV.

Nuclei	HF(SEI-I)			RMF(NL3)			Expt. [3]	
	S_n	S_{2n}	ε_n	S_n	S_{2n}	ε_n	S_n	S_{2n}
^{6}He	1.830	4.141	4.685	0.64	− 0.114	2.465	1.864 ± 0.001	0.974 ± 0.001
^{11}Li	1.630	1.096	3.882	1.922	4.217	3.732	0.330 ± 0.030	0.300 ± 0.030
^{11}Be	4.078	14.453	5.489	2.551	9.697	3.894	0.504 ± 0.006	7.317 ± 0.006
^{15}C	3.017	11.357	2.591	1.371	10.315	2.566	1.218 ± 0.001	9.395 ± 0.018
^{19}C	2.306	4.767	2.259	2.727	5.343	3.263	0.160 ± 0.120	4.350 ± 0.210
^{22}C	3.616	5.755	2.876	2.527	4.438	3.782	1.450 ± 1.030	1.120 ± 0.920
^{23}O	4.282	9.395	4.596	3.975	10.161	4.270	2.740 ± 0.120	9.590 ± 0.100
^{31}Ne	0.409	3.736	0.417	0.105	4.613	1.639		

the Dirac spinors for the nucleons whose third component of isospin is denoted by τ_{3i}. g_s, g_ω, g_ρ, and $\frac{e^2}{4\pi} = \frac{1}{137}$ are the coupling constants for the linear terms of the σ, ω, and ρ mesons and photons, respectively. g_2 and g_3 are the parameters for the nonlinear terms of the σ meson. M, m_σ, m_ω, and m_ρ are the masses of the nucleons and the σ, ω, and ρ mesons, respectively. $\omega^{\mu\nu}$, $\vec{B}^{\mu\nu}$, and $F^{\mu\nu}$ are the field tensors for the V^μ, $\vec{R}^\mu$, and photon fields, respectively. The quadrupole moment deformation parameter β_2, rms radii, and binding energy are evaluated using the standard relations [18]. The nuclear density $\rho = \sum_{i=1}^{A} \psi_i^\dagger \psi_i$ is obtained by solving the equation of motion obtained from the above Lagrangian [18,20]. The values of the parameters for NL3 are given as [12] $g_s = 10.217, g_\omega = 12.868, g_\rho = 4.574, g_2 = -10.431$ (fm^{-1}), $g_3 = -28.885$, $M = 939$ MeV, $m_\sigma = 508.194$ MeV, $m_\omega = 782.501$ MeV, and $m_\rho = 763.0$ MeV.

III. CALCULATIONS AND RESULTS

A. Ground-state properties using RMF(NL3) and HF(SEI-I)

The ground-state properties like binding energy (B.E.), rms matter radius, charge radius, and β_2 deformation of some of the halo projectile and core of the projectiles, along with the C target, have been studied with the well-known RMF formalism with the NL3 parameters. These properties are also compared with the nonrelativistic Hartree-Fock formalism using the SEI with the SEI-I parameter along with the experimental observations wherever available. We also give the results for some of the known unbound nuclei like ^{5}He and ^{10}Li because of their involvement in the present core and the valence Glauber formalism.

1. Binding energy

The calculated values of the B.E. for the core of projectile nuclei are presented in Table I using the RMF(NL3) and nonrelativistic HF with the SEI-I parameters. The calculated values of the B.E. closely agree with the experimental observations [22,23]. In comparison the RMF(NL3) results have B.E. values slightly higher than those of the HF(SEI-I) results. The B.E. difference between the theoretical and experimental values are also listed in Table I. Examining the results of Table I, it can be inferred that both the formalisms are equally capable of reproducing the experimental data.

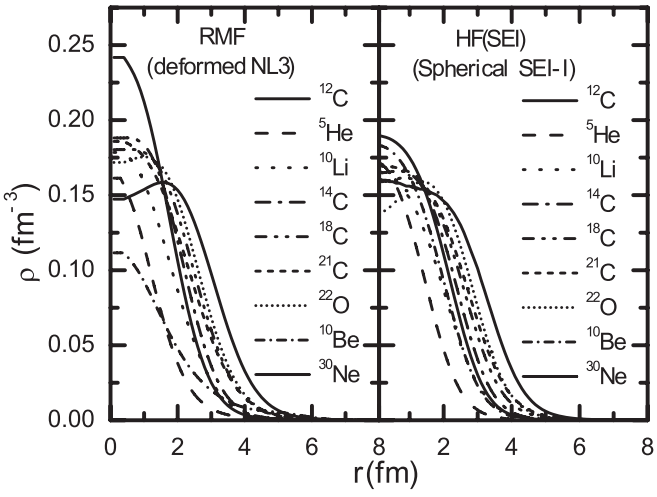

FIG. 1. The radial plots of densities from RMF(NL3) and HF(SEI-I) calculations of projectile (core) and target nuclei.

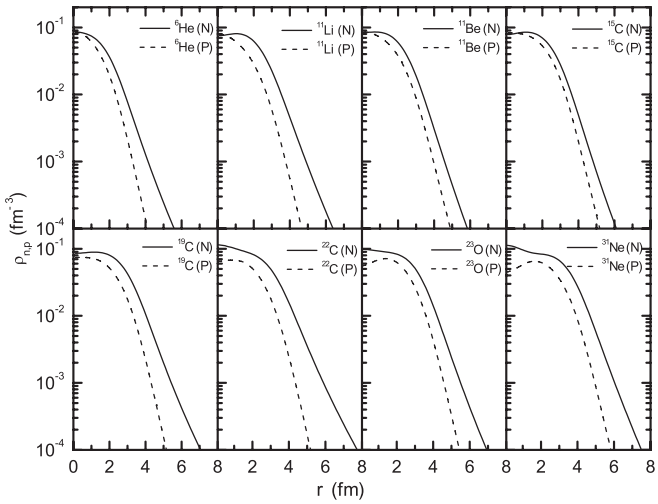

FIG. 2. The radial density plots of HF(SEI-I) calculations for projectile nuclei in logarithmic scale.

2. Nuclear radii and quadrupole deformation

The calculated rms matter radius and charge radius of projectile nuclei and core of the projectiles along with target nuclei from both relativistic RMF(NL3) and nonrelativistic HF(SEI-I) mean-field theories are presented in Table I. The experimental data are also given for comparison wherever available [24]. The rms proton radius r_p is obtained from the distribution of point protons inside the nucleus. The charge radius r_c is obtained by taking the finite size, 0.8 fm, of the proton, which is evaluated from the formula [20] $r_c = \sqrt{r_p^2 + 0.06}$. This table demonstrates the success of these

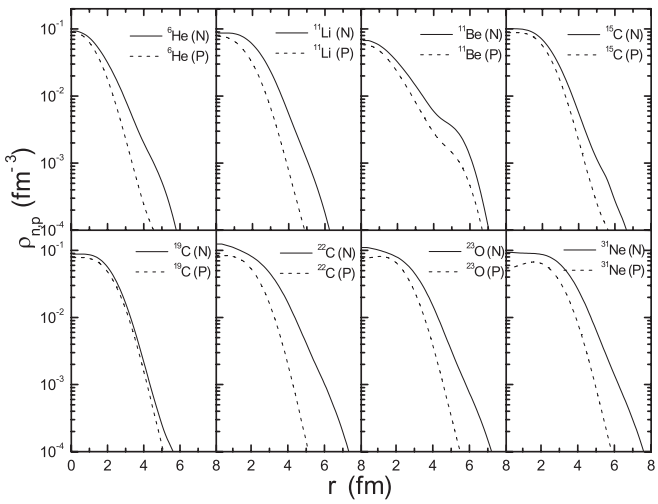

FIG. 3. Same as Fig. 2 but for the RMF(NL3) approximation.

TABLE III. The nucleon-nucleon cross section σ_{NN} and other parameters like α_{NN} and β_{NN} used to calculate the profile function.

E (MeV/A)	σ_{NN} (fm^2)	α_{NN}	β_{NN} (fm^2)
240	3.266 868	0.680 0303	0.097 843 707
730	4.174 130	−0.082 869 336	0.189 6611
800	4.260 00	−0.070 00	0.210 000
950	4.318 554	−0.207 8482	0.214 2974
960	4.319 103	−0.221 3738	0.213 4798
965	4.319 310	−0.228 1574	0.213 0555

theories in their predictions by showing the surprisingly comparable results.

Table I presents the quadrupole deformation parameter β_2 for halo projectiles and the core of the projectile systems obtained from the RMF model using the NL3 parameter set. The projectile nuclei in Table I are prolate in shape except for ^{19}C and ^{23}O (both have oblate deformations).

3. *One- and two-neutron separation energy*

The one (S_n) and two (S_{2n}) neutron separation energies of ^{6}He, ^{11}Li, ^{11}Be, ^{15}C, ^{19}C, ^{22}C, ^{23}O and ^{31}Ne halo nuclei are presented in Table II. These energies have been estimated as

$$S_n = \text{B.E}(N, Z) - \text{B.E}(N-1, Z) \tag{19}$$

and

$$S_{2n} = \text{B.E}(N, Z) - \text{B.E}(N-2, Z). \tag{20}$$

The calculated values of separation energies S_n and S_{2n} for halo nuclei obtained by both the formalisms HF(SEI-I) and RMF(NL3) are compared with the experimental observations. The small value of S_n energy for ^{11}Be, ^{15}C, ^{19}C, ^{23}O, and ^{31}Ne nuclei from their S_{2n} values are the primary indications of their one-neutron halo candidature. Table II also presents the single-particle energy state of the last occupied neutron (ε_n) of the considered halo nuclei from both the formalisms.

4. *Nuclear densities*

The densities of ^{12}C, ^{5}He, ^{10}Li, ^{10}Be, ^{14}C, ^{18}C, ^{20}C, ^{22}O, and ^{30}Ne nuclei are obtained from axially deformed RMF(NL3) and spherical HF(SEI-I) theories. These axially deformed densities are converted into their spherical equivalent and presented in Fig 1. Figure 1 (left panel) shows the spherical equivalent of the deformed RMF(NL3) density. The right panel of this figure shows the spherical density obtained from the HF(SEI) formalism with SEI-I interaction parameters [10]. We find almost similar densities from both RMF and nonrelativistic mean-field approximations with SEI. Some exceptions are seen in Fig. 1 for ^{12}C, ^{10}Be, and ^{30}Ne nuclei. In the case of RMF(NL3) the density of ^{12}C shows a stiff hike in the central portion and a sudden fall in the tail part. On the other hand the behavior of ^{10}Be is the opposite. The density distribution of ^{30}Ne shows a small depression at the center indicating the structure of a bubble nucleus. The same effect appeared to a small extent in ^{22}O from both systems of densities, similar to our earlier calculations [25].

Figures 2 and 3 show the proton and neutron density distributions for projectiles as a function of radial distance of the considered halo nuclei. Similar trends have appeared in the density distribution of these nuclei for both RMF(NL3) and HF(SEI-I) densities as seen in Figs. 2 and 3. The extension of neutron density distributions are seen as compared to the proton distributions. This may be because the neutron to proton ratio is more than 1. The longer tail appeared in neutron density distribution as compared to the proton density distribution signify its neutron halo nature of these nuclei.

5. *Various inputs for the Glauber model*

One of the inputs for the evaluation of the profile function in the Glauber model is the energy-dependent parameters σ_{NN}, α_{NN}, and β_{NN}, where σ_{NN} is the total nuclear reaction cross section of a NN collision, α_{NN} is the ratio of the real part to the imaginary part of the forward nucleon-nucleon scattering amplitude, and β_{NN} is the slope parameter, which determines the fall of the angular distribution of the NN scattering. Table III presents these energy-dependent parameters for various energy ranges. These parameters have been estimated by using spline interpolation as suggested in Ref. [26].

The most important input in the Glauber model formalism is the densities of the projectile and the target. The computer code used here cannot use the density directly [14]. So, we convert the densities into a Gaussian form and calculate the

TABLE IV. The Gaussian coefficients for the projectile (core) and target with RMF(NL3) and HF(SEI-I) densities.

Nuclei	RMF(NL3)				HF(SEI-I)			
	c_1	a_1	c_2	a_2	c_1	a_1	c_2	a_2
^{12}C	−0.159 36	0.632 931	0.415 315	0.304 586	−3.800 28	0.361 705	3.984 36	0.345 456
^{5}He	−1.209 18	0.363 434	1.405 51	0.363 380	−0.117 28	0.689 757	0.294 53	0.414 845
^{10}Li	−1.1064	0.329 244	1.282 38	0.303 979	−1.692 25	0.363 722	1.861 98	0.337 186
^{10}Be	−1.23 458	0.185 387	1.376 85	0.185 291	−3.365 76	0.379 683	3.547 75	0.363 577
^{14}C	−0.433 794	0.449 739	0.623 356	0.291 956	−1.886 75	0.342 428	2.045 96	0.308 693
^{18}C	−1.219 10	0.279 772	1.378 17	0.243 514	−1.942 06	0.291 905	2.098 75	0.263 030
^{21}C	−1.187 02	0.252 476	1.410 22	0.225 988	−3.993 17	0.249 448	4.160 38	0.238 052
^{22}O	−4.064 57	0.272 853	4.232 98	0.257 118	−2.568 38	0.269 287	2.699 32	0.244 516
^{30}Ne	−3.6109	0.221 938	3.743 09	0.206 388	−2.050 83	0.198 501	2.194 28	0.180 662

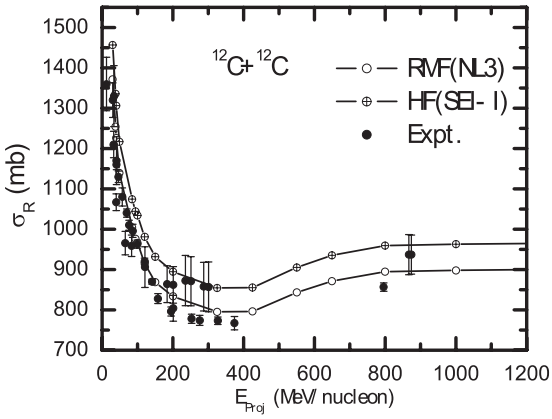

FIG. 4. The total nuclear reaction cross section σ_R as a function of projectile energy. The results obtained from RMF(NL3) and HF(SEI-I) densities are compared with experimental data [14,26].

Gaussian coefficients c_i and a_i using the following relation:

$$\rho(r) = \sum_{i=1}^{n} c_i \exp[-a_i r^2]. \quad (21)$$

The Gaussian coefficients that are used as inputs in the Glauber model code are listed in Table IV for both RMF(NL3) and HF(SEI-I) interactions.

B. Total reaction cross sections

Figure 4 presents the variation of total nuclear reaction cross sections for $^{12}C + ^{12}C$ as a function of projectile energy over the range of 30–1200 MeV/A. The σ_R obtained from RMF density up to the range of ∼30–120 MeV/A excellently reproduce the experimental data. Beyond this value of the projectile energy, σ_R have slightly greater values. The σ_R values calculated with HF(SEI-I) are a little bit higher than those calculated with RMF(NL3). The reaction cross sections σ_R obtained by both the formalisms have reasonable values, which compare well with the experimental observations.

Some results of our calculations are listed in Table V for different projectiles with a ^{12}C target. The reaction cross section σ_R obtained using the NL3 and SEI-I densities are in agreement with the experimental data. A further inspection of the comparison reveals overall the superiority of the SEI-I density over the NL3 density. It may be noted that the microscopic density obtained from RMF theory with the NL3 set is quite successful for various applications including the nuclear reaction cross section calculations [28] throughout the periodic chart. In some of our earlier calculations, it is shown that σ_R obtained with the NL3 set is superior to that obtained with the microscopic nonrelativistic SkI4 Skyrme force [11]. However, it is remarkable to mention here that the SEI-I density performs even better than the NL3 density for the estimation of reaction cross sections for the chosen halo nuclei. Thus the present calculations encouraged us to use the SEI density in future calculations for the analysis of nuclear reactions.

TABLE V. Total nuclear reaction cross section for various projectiles with a ^{12}C target. The experimental data [27] are given for comparison.

Projectile	Energy	σ_R (mb)		
	(MeV/A)	RMF(NL3)	SEI(SEI-I)	Expt.
^{6}He	800	721	740	722 ± 6
^{11}Li	800	930	944	1060 ± 10
^{11}Be	950	1038	932	942 ± 8
^{15}C	730	995	1054	945 ± 10
^{19}C	960	1187	1202	1231 ± 28
^{23}O	960	1242	1308	1308 ± 16
^{31}Ne	240	1361	1465	1435 ± 22

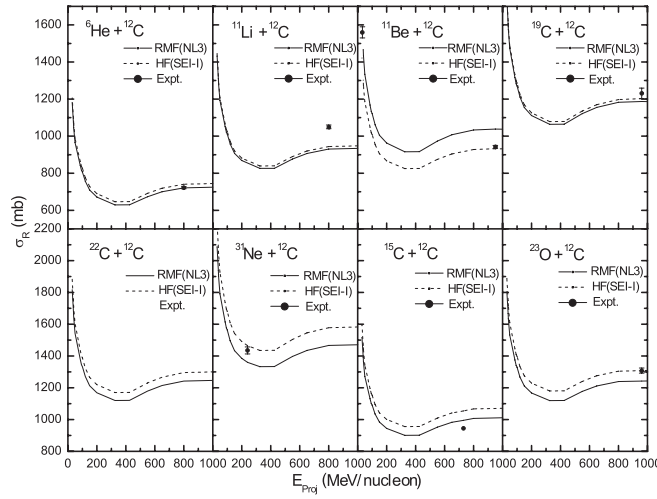

FIG. 5. Reaction cross sections with different projectile energies, E_{proj}, for ^{6}He, ^{11}Li, ^{11}Be, ^{19}C, ^{22}C, and ^{31}Ne with a ^{12}C target. The experimental data are given for comparison wherever available [27].

Figure 5 shows the total reaction cross section as a function of the projectile energy for ^{6}He, ^{11}Li, ^{11}Be, ^{19}C, ^{22}C, and ^{31}Ne halo nuclei over a wide range of energy, 30–1000 MeV/A. The value of σ_R is observed to be larger at small incident energy and to start decreasing with the increase of E_{proj} up to ∼300 MeV/A. A slight increase in σ_R is seen (Fig. 5) for 300–750 MeV/A and σ_R becomes almost independent of E_{proj} beyond 750 MeV/A. The values of σ_R with SEI-I are slightly greater than the NL3 results except from the ^{11}Be channel, and the overall comparison with experimental data is better for SEI-I as compared to NL3.

IV. SUMMARY AND CONCLUSION

In summary, we have presented here some ground-state properties and reaction cross sections for ^{6}He, ^{11}Li, ^{11}Be, ^{15}C, ^{19}C, ^{22}C, ^{23}O, and ^{31}Ne (some of the halo nuclei) projectiles with a ^{12}C target using the densities of relativistic and nonrelativistic mean-field formalisms. These densities are obtained from completely different sources, which are used in the Glauber model approach for the evaluation of σ_R. In general, the results obtained with both the RMF and HF formalisms compare well with the experimental data with an

edge of the density obtained from the SEI-I interaction. The use of the SEI-I density will be of further interest to analyze reaction dynamics and structural effects for other reactions involving halo nuclei.

ACKNOWLEDGMENTS

M.K.S. thanks the Institute of Physics, Bhubaneswar, and SPMS, Thapar University, Patiala, for their kind hospitality.

[1] I. Tanihata, H. Hamagaki, O. Hashimoto, Y. Shida, N. Yoshikawa, K. Sugimoto, O. Yamakawa, T. Kobayashi, and N. Takahashi, Phys. Rev. Lett. **55**, 2676 (1985); J. Phys. G **22**, 661 (1996).
[2] I. Tanihata *et al.*, Phys. Lett. B **287**, 307 (1992).
[3] A. Ozawa *et al.*, Nucl. Phys. A **691**, 599 (2001).
[4] I. Hamamoto, Phys. Rev. C **81**, 021304 (2010); Y. Urata, K. Hagino, and H. Sagawa, *ibid.* **83**, 041303(R) (2011); K. Minomo, T. Sumi, M. Kimura, K. Ogata, Y. R. Shimizu, and M. Yahiro, *ibid.* **84**, 034602 (2011).
[5] S. K. Patra and C. R. Praharaj, Phys. Lett. B **273**, 13 (1991).
[6] K. Tanaka *et al.*, Phys. Rev. Lett. **104**, 062701 (2010).
[7] N. Kobayshi *et al.*, arXiv:1111.7196.
[8] A. Ozawa, T. Kobayashi, T. Suzuki, K. Yoshida, and I. Tanihata, Phys. Rev. Lett. **84**, 5493 (2000).
[9] I. Tanihata *et al.*, Nucl. Phys. A **682**, 114c (2001).
[10] B. Behera, X. Viñas, M. Bhuyan, T. R. Routray, B. K. Sharma, and S. K. Patra (unpublished); M. Bhuyan, T. R. Routray, S. K. Singh, S. K. Patra, and X. Viñas (unpublished).
[11] M. K. Sharma, M. S. Mehta, and S. K. Patra, Int. J. Mod. Phys. E **22**, 1350005 (2013).
[12] G. A. Lalazissis, J. König, and P. Ring, Phys. Rev. C **55**, 540 (1997).
[13] R. J. Glauber, Phys. Rev. **100**, 242 (1955); in *Lectures in Theoretical Physics*, edited by W. E. Brittin and L. C. Dunham (Interscience, New York, 1959), Vol. 1, p. 315.
[14] B. Abu-ibrahim, Y. Ogawa, Y. Suzuki, and I. Tanihata, Comput. Phys. Commun. **151**, 369 (2003).
[15] P. J. Karol, Phys. Rev. C **11**, 1203 (1975).
[16] J. Chauvin, D. Lebrun, A. Lounis, and M. Buenerd, Phys. Rev. C **28**, 1970 (1983).
[17] P. Ring, Prog. Part. Nucl. Phys. **37**, 193 (1996).
[18] W. Pannert, P. Ring, and J. Boguta, Phys. Rev. Lett. **59**, 2420 (1987).
[19] J. Baguta and A. R. Bodmer, Nucl. Phys. A **292**, 413 (1977).
[20] S. K. Patra and C. R. Praharaj, Phys. Rev. C **44**, 2552 (1991).
[21] M. Del Estal, M. Centelles, X. Vinas, and S. K. Patra, Phys. Rev. C **63**, 024314 (2001).
[22] G. Audi, A. H. Wapstra, and C. Thibault, Nucl. Phys. A **729**, 337 (2003).
[23] M. Wang, G. Audi, A. H. Wapstra, F. G. Kondev, M. MacCormick, X. Xu, and B. Pfeiffer, Chinese Phys. C **36**, 1603 (2012).
[24] C. W. De Jager, H. De Vries, and C. De Vries, At. Data Nucl. Data Tables **14**, 479 (1974); I. Angeli, *ibid.* **87**, 185 (2004).
[25] A. Shukla, Sven Åberg, and S. K. Patra, J. Phys. G **38**, 095103 (2011).
[26] W. Horiuchi, Y. Suzuki, B. Abu-Ibrahim, and A. Kohama, Phys. Rev. C **75**, 044607 (2007).
[27] B. Abu-Ibrahim and Y. Suzuki, Phys. Rev. C **61**, 051601 (2000); M. Fukuda *et al.*, Phys. Lett. B **268**, 339 (1991); A. Ozawa *et al.*, Nucl. Phys. A **691**, 599 (2001); T. Kobayashi *et al.*, Phys. Lett. B **232**, 51 (1989); I. Tanihata *et al.*, *ibid.* **206**, 592 (1988); M. Takachi *et al.*, Nucl. Phys. A **834**, 412c (2010).
[28] A. Shukla, B. K. Sharma, R. Chandra, P. Arumugam, and S. K. Patra, Phys. Rev. C **76**, 034601 (2007); S. K. Patra, R. N. Panda, P. Arumugam, and R. K. Gupta, *ibid.* **80**, 064602 (2009).